

A surface mechanism for O₃ production with N₂ addition in dielectric barrier discharges

Mackenzie Meyer¹ , John Foster²  and Mark J Kushner^{1,*} 

¹ Electrical Engineering and Computer Science Department, University of Michigan, 1301 Beal Ave., Ann Arbor, MI 48109-2122, United States of America

² Nuclear Engineering & Radiological Sciences Department, University of Michigan, 2355 Bonisteel Blvd., Ann Arbor, MI 48109-2104, United States of America

E-mail: mjkush@umich.edu

Received 10 May 2023, revised 1 July 2023

Accepted for publication 20 July 2023

Published 4 August 2023



CrossMark

Abstract

Ozone, O₃, is a strong oxidizing agent often used for water purification. O₃ is typically produced in dielectric barrier discharges (DBDs) by electron-impact dissociation of O₂, followed by three-body association reactions between O and O₂. Previous studies on O₃ formation in low-temperature plasma DBDs have shown that O₃ concentrations can drop to nearly zero after continued operation, termed the ozone-zero phenomenon (OZP). Including small (<4%) admixtures of N₂ can suppress this phenomenon and increase the O₃ production relative to using pure O₂ in spite of power deposition being diverted from O₂ to N₂ and the production of nitrogen oxides, N_xO_y. The OZP is hypothesized to occur because O₃ is destroyed on the surfaces in contact with the plasma. Including N₂ in the gas mixture enables N atoms to occupy surface sites that would otherwise participate in O₃ destruction. The effect of N₂ in ozone-producing DBDs was computationally investigated using a global plasma chemistry model. A general surface reaction mechanism is proposed to explain the increase in O₃ production with N₂ admixtures. The mechanism includes O₃ formation and destruction on the surfaces, adsorption and recombination of O and N, desorption of O₂ and N₂, and NO_x reactions. Without these reactions on the surface, the density of O₃ monotonically decreases with increasing N₂ admixture due to power absorption by N₂ leading to the formation of nitrogen oxides. With N-based surface chemistry, the concentrations of O₃ are maximum with a few tenths of percent of N₂ depending on the O₃ destruction probability on the surface. The consequences of the surface chemistry on ozone production are less than the effect of gas temperature without surface processes. An increase in the O₃ density with N-based surface chemistry occurs when the surface destruction probability of O₃ or the surface roughness was decreased.

Keywords: ozone production, ozone-zero phenomenon, dielectric barrier discharge, plasma modeling

(Some figures may appear in colour only in the online journal)

* Author to whom any correspondence should be addressed.



Original content from this work may be used under the terms of the [Creative Commons Attribution 4.0 licence](https://creativecommons.org/licenses/by/4.0/). Any further distribution of this work must maintain attribution to the author(s) and the title of the work, journal citation and DOI.

1. Introduction

Ozone, O₃, is widely used in commercial and municipal settings for purification of water [1–3]. The generation of O₃ for water purification is typically accomplished using a low-temperature plasma device, often in a pulsed dielectric barrier discharge (DBD) configuration, where one or both electrodes are coated with a dielectric. DBDs are typically operated in pure O₂ to maximize O₃ production. O₃ is produced from O₂ through a two-step process. Electron-impact dissociation of O₂ produces O atoms, followed by the production of O₃ by a third body mediated reaction, $O + O_2 + M \rightarrow O_3 + M$. Production of O₃ decreases in the plasma at elevated gas temperatures due to endothermic processes which destroy the ozone and reduction in the rates of 3-body processes.

In addition to reactions in the plasma, reactions can occur between O₃ and surfaces in contact with the plasma. Itoh *et al* showed that O₃ could be lost in reactions with the surfaces and that the rate of loss depended on the metal electrode material [4]. Yanallah *et al* simulated O₃ production and showed that including O₃ loss reactions on the surfaces changed the electrical characteristics of the discharge [5]. Mazánková *et al* exposed copper and aluminum surfaces to O₃ produced by an ozonizer to study surface composition [6]. They showed that the elemental O composition of those surfaces increased after exposure to O₃.

The production of O₃ in many commercial DBD reactors is not constant over time. After a long period of operation, the flow rate of O₃ leaving the reactor sometimes drops to nearly zero. This phenomenon was coined the ozone-zero phenomenon (OZP) by Taguchi *et al* [7]. OZP does not imply that O₃ is not being produced inside the reactor. Instead, OZP refers to the O₃ observed leaving the reactor. The time over which the OZP occurs is much longer than a gas residence time. Taguchi *et al* proposed that the primary cause of OZP was destruction of O₃ on the surfaces in contact with the plasma due to long term changes in the properties of the surface as opposed to a volumetric process, either a decrease in production or increase in destruction, occurring within the plasma. The rationale is plasma processes should scale with the gas residence time.

The OZP was reproduced by Murayama *et al* [8]. Auger emission spectroscopy of the electrodes showed that O atoms penetrated the stainless-steel electrode over time and changed the properties of the electrode, possibly contributing to the OZP. Taguchi *et al* showed that the OZP was dependent on the power per electrode area (W·cm⁻²) [9]. The rate of the decrease in O₃ concentration was higher at larger values of specific power. Recovery from the OZP was shown to occur with continued operation of the reactor. Itoh *et al* showed the surface of the stainless-steel electrode was oxidized by O₃ and O [10].

The OZP can be suppressed by the addition of nitrogen-containing species into the discharge, in spite of the diversion of power deposition from O₂ into the nitrogen-containing additives and formation of N_xO_y species. Early work by Taguchi *et al* showed that adding 0.2% N₂ to pure O₂ DBDs suppressed the OZP and increased the O₃ concentration

relative to a baseline of 0.01% N₂ [7]. They hypothesized that NO₂ formed from NO or N₂ in the feed gas aided in the recovery of the OZP. Itoh *et al* also showed that the OZP was suppressed with a N₂ addition of 0.2% [10]. Seyrling *et al* confirmed that the addition of N₂ (2.3% by weight) could suppress the OZP [11]. They also showed that after the N₂ flow was stopped, the O₃ generation efficiency declined at a much slower rate compared to experiments with no N₂ flow over time scales much longer than the gas residence time. This indicated that the process by which N₂ suppresses the OZP was not a volumetric process but instead a slowly evolving process on the surface. They also showed that the total amount of N₂ added was the dominant factor in determining the rate of decrease in O₃ efficiency.

In following work, Seyrling *et al* examined N₂O and N₂O₅ concentrations to further investigate the OZP suppression [12]. While both N₂O and N₂O₅ were present when N₂ was flowing, only N₂O₅ was present after the flow of N₂ was turned off. They proposed that N₂O₅ adsorbs onto sputter products on the surface of the stainless-steel electrodes. Qin *et al* showed that 4% N₂ in a packed bed DBD increased the O₃ concentration [13]. As the average electric field/gas number density, E/N, in the reactor increased in the packed bed reactor, the admixture of N₂ producing the largest O₃ concentration decreased.

In this paper, we discuss results from a computational investigation in which a general surface reaction mechanism is proposed to explain increased O₃ concentration with the addition of N₂ to O₂ DBDs. The surface reaction mechanism includes formation and destruction of O₃, adsorption and recombination of N and O, desorption of O₂ and N₂, and reactions forming or consuming NO_x species. While some probabilities for these surface reactions were taken from the literature for borosilicate glass, a dielectric material commonly used in DBDs, many probabilities in the reaction mechanism were estimated to explain why O₃ density can be a maximum at a nonzero N₂ admixture in spite of power being diverted from O₂ to N₂. This surface reaction mechanism was implemented in a zero-dimensional (0D) plasma chemistry model *GlobalKin*.

First, the plasma properties and O₃ production were examined without reactions on the surface. With 0.2% N₂ in O₂, the dominant reactive oxygen and nitrogen species (RONS) were O, N, O₃, NO, NO₂, NO₃, N₂O, and N₂O₅. Without the surface reaction mechanism, O₃ density monotonically decreased as the N₂ admixture increased. An increase in gas temperature results in a decrease in O₃ density. With the surface reaction mechanism, O₃ concentrations decreased relative to O₃ without the surface reactions due to there being a finite probability of O₃ destruction on the surface. However, the O₃ density with the surface reaction mechanism is a maximum with 0.2% N₂ addition compared to otherwise pure O₂. This favorable influence of N₂ is due to N adsorption occupying sites that would otherwise be available for O₃ destruction. The O₃ density also decreases as the probability of destruction on the surface increases and as the surface roughness increases.

The global plasma chemistry model and the reaction mechanism are described in section 2. In section 3, formation of O₃ without reactions on the surface is examined, including

for varying N_2 admixtures (section 3.1) and gas temperatures (section 3.2). The formation of O_3 with the surface reaction mechanism, including destruction of O_3 , is discussed in section 4. The variations in O_3 density with N_2 admixture (section 4.1), surface destruction probability (section 4.2), and surface roughness (section 4.3) are also discussed. Finally, concluding remarks are in section 5.

2. Description of the model

The model used in this work is *GlobalKin*, described in detail in [14]. *GlobalKin* is a 0D plasma chemistry model representing the plasma as a well-stirred reactor. Densities are solved by integrating continuity equations for each species. Electron-impact, ion-molecule and heavy particle reactions, diffusion to surfaces, and flow into and out of the system comprise the sources and losses in the continuity equations. The electron and gas temperatures are solved using their respective energy equations. The electron energy distribution is obtained by solving Boltzmann's equation in the steady state. From the electron energy distributions for a range of E/N (electric field/gas number density), a lookup table of electron-impact rate coefficients for different electron temperatures (mean electron energy) is generated.

The surface kinetics module (SKM), a module in *GlobalKin* [15, 16], is a surface site balance model that produces the occupancy of surface sites. The surface site occupancy θ of species i is determined by

$$\frac{d\theta_i}{dt} = \sum_{j,k} \theta_k \Gamma_j p_{ijk} + \sum_{k,l} \theta_k \theta_l p'_{ikl} - \theta_i \left(\sum_j \Gamma_j p_{ji} + \sum_k \theta_k p'_{ik} \right). \quad (1)$$

The first term is the source of species i from reactions between species k on the surface and flux Γ_j of gas phase species j with a probability of reaction p_{ijk} . The second term is a source of species i from reactions between two surface species, k and l , with probability p'_{ikl} . The last term is the loss of species i due to reactions with both gas phase and surface species. Unless otherwise noted, the total surface site density is 10^{15} sites cm^{-2} . Using a time-slicing technique, the SKM is integrated for times greater than that between calls to the SKM, allowing the surface species to reach a steady state at a rate commensurate with the gas phase species. In this work, the SKM is called every 50 ns and integrated for 1 ms on each call.

The flux to the surface, appearing in equation (1), is provided using a diffusion length and the reactor averaged density resulting from the global model,

$$\Gamma_{jk} = N_j D_j / \Lambda_k. \quad (2)$$

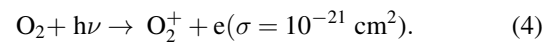
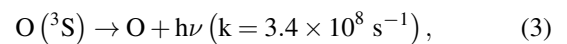
In equation (2), Γ_{jk} is the flux of species j to surface k in contact with the plasma, N_j is the volume averaged density of species j , and D_j is its diffusion coefficient. Λ_k is the diffusion length for transport to surface k . In typical DBDs, as addressed here, the axial dimension in the plasma between electrodes or

materials covering the electrodes is small compared to the lateral length. As a result, diffusive fluxes to those surfaces dominate. For charged species, D_j is the species modified ambipolar diffusion coefficient.

The geometry modeled in *GlobalKin* is a DBD with a high surface-to-volume ratio, having a plasma volume of $4.4 \text{ cm} \times 4.4 \text{ cm} \times 300 \text{ } \mu\text{m}$. The pressure is 1 atm and the flow rate is 2 slm producing a residence time of 16 ms. The electrodes in the DBD are covered with borosilicate glass, chosen as a representative dielectric. The DBD operated with a pulse length of 130 ns (20 ns ramp up and 30 ns ramp down) and peak power of 5 kW, which produces an energy-per-pulse of 0.625 mJ or 1.1 mJ cm^{-3} . The pulse repetition rate is 10 kHz (10^{-4} s period) which corresponds to average power of 6.25 W or 10.8 W cm^{-3} . 150 ms (1500 pulses) were modeled in *GlobalKin* to achieve a pulse-periodic steady state. This gas phase integration time corresponds to approximately 50 min of operation for surface processes. In the base case, the inlet gas temperature and wall temperatures are held at 300 K. The electron temperature T_e is calculated during the power pulse and is set to 0.025 eV after the pulse when power is removed.

The operation of typical DBDs relies on the propagation of streamers, or highly localized filaments of plasma. To resolve streamers, a 2D or 3D modeling approach is required. However, performing 2D or 3D simulations for thousands of pulses, which is needed to track the evolution of surface properties, is prohibitively computationally expensive. The use of a global model which addresses reactor average properties enables investigation of many pulses over long periods. As discussed below, this approximation applies provided dominant processes are not non-linear.

The DBD operates in otherwise pure O_2 with admixtures of N_2 . The base case simulates the plasma formed in 0.2% N_2 (99.8% O_2). The gas phase reaction mechanism is adapted from Van Gaens and Bogaerts [17]. Additions for excited states of O beyond $O(^1D)$ were made [18–24]. The species considered are listed in table 1 — 43 species are included with 15 charged species. O_3^* , a vibrationally excited state of O_3 was not included in this study. 1 photon species emitted from $O(^3S)$ is considered, and its reactions are



685 reactions in the gas phase are included in the mechanism.

The proposed surface reaction mechanism is listed in table 2. The reaction mechanism was developed with the goal of explaining the increase in O_3 density at low admixtures of N_2 in the presence of surface reactions that include destruction of O_3 . The reaction mechanism considers physisorbed species. The surface reaction mechanism includes O_3 destruction by dissociative adsorption of O_3 on a bare wall site, W_s , to produce adsorbed O_s ,

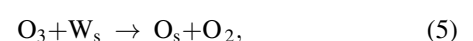


Table 1. Species included in the reaction mechanism.

Charged Species	e, O ₂ ⁺ , O ₂ ⁻ , O ₄ ⁺ , O ⁺ , O ⁻ , O ₃ ⁻ N ₂ ⁺ , N ₃ ⁺ , N ₄ ⁺ , N ⁺ NO ⁺ , NO ₂ ⁺ , NO ₂ ⁻ , NO ₃ ⁻
Neutral Species	O ₂ , O, O ₃ N ₂ , N NO, NO ₂ , NO ₃ , N ₂ O, N ₂ O ₃ , N ₂ O ₄ , N ₂ O ₅
Excited states	O ₂ (v), O ₂ (r), O ₂ (¹ Δ _g), O ₂ (¹ Σ _u), O(¹ D), O(¹ S), O(⁵ S), O(³ S), O(⁵ P) N ₂ (r), N ₂ (v), N ₂ (A ³ Σ _u), N ₂ (a ¹ Σ), N(² D) N ₂ O(v)

Table 2. Surface reaction mechanism.

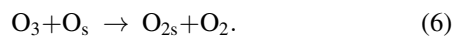
Reaction	Rate (probability unless otherwise specified)	Note
O ₃ + W _s → O _s + O ₂	0.01	a
O ₃ + O _s → O _{2s} + O _s	0.01	a
O + W _s → O _s	0.7	[35]
O + O _s → W _s + O ₂	0.002	[27, 28]
O _s + O _s → W _s + O _{2s}	1.0 × 10 ⁻¹⁸ cm ² s ⁻¹	a
O ₂ + O _{2s} → O ₂ + O ₂ + W _s	0.002	a
O ₂ + O _s → W _s + O ₃	0.004	[36]
N + W _s → N _s	0.7	b
N + N _s → W _s + N ₂	0.002	b
N _s + N _s → W _s + N _{2s}	1.0 × 10 ⁻¹⁸ cm ² s ⁻¹	b
O ₂ + N _{2s} → N ₂ + O ₂ + W _s	0.002	a
NO + O _s → W _s + NO ₂	10 ⁻⁸	[29]
O ₂ + N _s → O _s + NO	10 ⁻⁸	a, c
O + N _s → W _s + NO	10 ⁻⁸	a,c
N + O _s → W _s + NO	10 ⁻⁸	a,c
NO + N _s → O _s + N ₂	10 ⁻⁸	a,c
NO ₂ + N _s → O _{2s} + N ₂	10 ⁻⁸	a,c
NO ₂ + N _s → W _s + NO + NO	10 ⁻⁸	a,c
NO ₂ + N _s → O _s + N ₂ O	10 ⁻⁸	a,c
NO ₃ + N _s → W _s + NO ₂ + NO	10 ⁻⁸	a,c

^a Rate is estimated.

^b Based on analogy to O_s.

^c Reaction is based on analogous gas phase reaction.

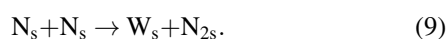
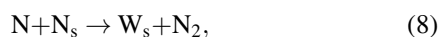
followed by dissociative desorption by reaction of O₃ with that surface site,



(The subscript s denotes a surface species.) These reactions for O₃ destruction have been proposed by several researchers [6, 13, 25]. As will be discussed in section 4, W_s is more abundant than O_s and is therefore responsible for the majority of O₃ destruction on the surface. N is adsorbed by

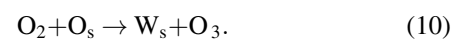


consuming a W_s site. This reaction enables N_s to block sites that are otherwise available for O₃ destruction by reaction 5. N desorbs both through Eley-Rideal (reaction 8) and Langmuir-Hinshelwood (reaction 9) mechanisms by

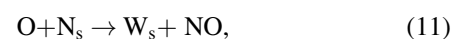


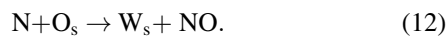
N_{2s} is loosely physisorbed which is then removed from the surface by collisions of O₂ with the surface. Similarly, O adsorbs and desorbs through analogous reactions to N. The probabilities of O and N recombination on surfaces can vary widely depending on the surface material. Dielectric surfaces, as investigated here, typically have lower surface recombination probabilities than metal surfaces. For example, in Stafford *et al*, a recombination probability of 0.13 was reported for stainless steel during initial plasma exposure [26], while on dielectric surfaces, a recombination probability of 0.002 was reported [27, 28].

O_s is additionally removed through O₃ formation on the surface by

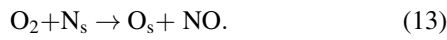


Other mechanisms of O_s and N_s removal involve formation or destruction of N_xO_y species. NO is formed through O and N association by

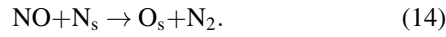




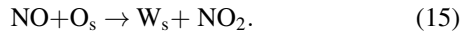
NO is also formed by O_2 reacting with adsorbed N_s by



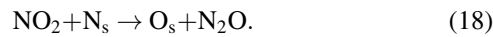
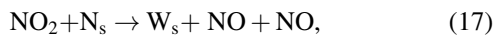
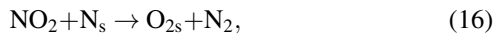
NO is destroyed through N_2 formation by



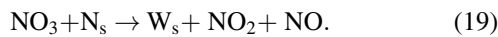
NO forms NO_2 by



NO_2 reacts with N_s , forming several products by



NO_3 is reduced to form NO and NO_2 by



Where available from the literature, reaction probabilities for surface reactions were selected for borosilicate glass. Otherwise, the probabilities of reactions were estimated to explain the increase in O_3 density at low N_2 admixtures that is observed experimentally. The reactions that involve NO_x species have a probability of 10^{-8} , based on the probability for reaction 15 discussed in [29].

Borosilicate glass was chosen due to the availability of reaction probabilities. As mentioned above, other materials, either dielectric (e.g., quartz) or metallic, will quantitatively have different reaction probabilities. However, while the probabilities will differ between different materials, the same general conclusions apply. To extend the surface mechanism to other materials, the general sequence of O_3 quenching and N atom adsorption blocking quenching sites should apply.

Destruction of O_3 does not occur on the surface when the SKM is not executed. In the absence of the surface reaction mechanism employed in the SKM, the only surface reactions are quenching of excited states and recombination of charged particles and atomic species.

3. O_3 formation in a pulsed DBD

In this section, plasma properties and RONS densities without the surface reaction mechanism are discussed for a 0.2% N_2 admixture into otherwise pure O_2 with an inlet gas temperature of 300 K. The gas temperature in the discharge was allowed to vary, but the gas temperature increased by less than 2 K over the entire simulation. The variation of the O_3 density with N_2 admixture, as well as gas temperature, are examined in sections 3.1 and 3.2.

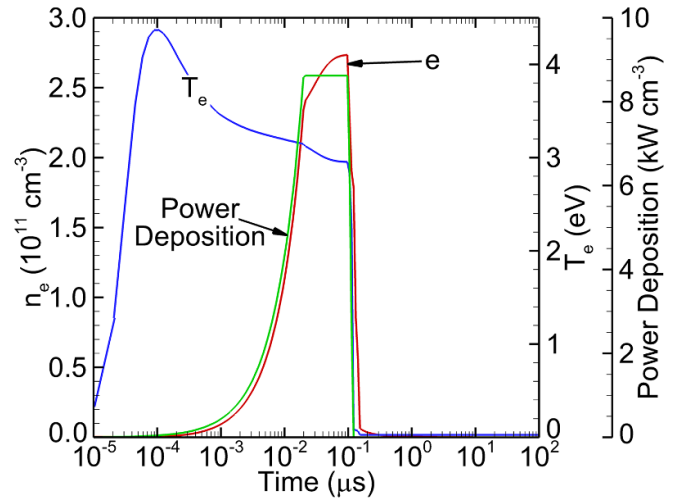


Figure 1. Plasma properties over the last pulse for the O_2 DBD with 0.2% N_2 . Reactions on the surface are not included.

Electron density, electron temperature T_e , and the power deposition over the last discharge pulse (1500th pulse at 10 kHz) are shown in figure 1. T_e increases early during the power pulse, reaching a maximum of 4.4 eV at 0.1 ns. This increase in T_e enables avalanching of electrons by electron-impact ionization. The power continues ramping up over 20 ns, leading to a corresponding increase in electron density. The increase in electron density allows T_e to decrease while still dissipating the specified power. The power reaches a steady state of 5 kW (8.6 kW cm^{-3}). The electron density continues to increase, and T_e continues to decrease, over the duration of the pulse as population of excited states enables more efficient multi-step ionization. The electron density reaches $2.7 \times 10^{11} \text{ cm}^{-3}$ before the power ramps down at which time the electron density and T_e both decrease quickly. The electron density is less than 1% of the maximum by 280 ns, or 150 ns after the pulse has terminated. The decrease in electron density following the pulse is dominated by electron attachment to O_2 forming O_2^- .

The electron and radical densities discussed here are volume averages, as this is the outcome and limitation of global models. These values may be low compared to peak densities that occur in localized streamers. These global model derived densities should closely approximate the volume average of these quantities in a streamer dominated discharge provided that non-linear processes do not dominate. For example, multi-step ionization is a process that scales non-linearly with electron density. In short pulse, atmospheric pressure plasmas, excitation and ionization tend to be dominated by collisions with ground state species. Ozone formation is sensitive to gas temperature (decreasing efficiency with increasing pressure). The higher specific power deposition in a streamer will produce a locally higher gas temperature. However, thermal conduction from the narrow streamers (a few hundred microns) to the bulk gas and to the electrodes quickly equilibrate the temperature.

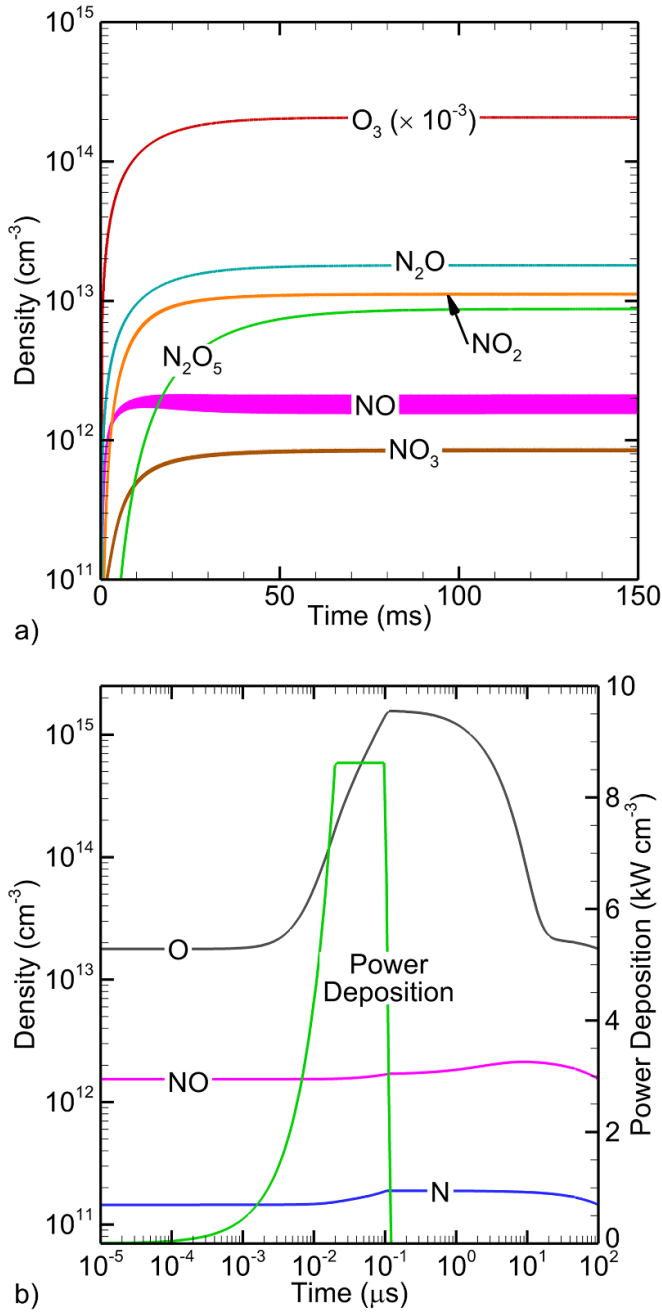
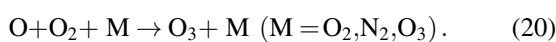
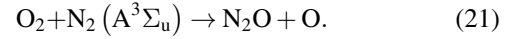


Figure 2. Reactive species densities for the O_2 DBD with 0.2% N_2 . (a) Long-lived species and (b) short-lived species. Reactions on the surface are not included.

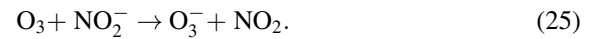
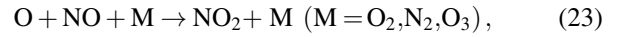
RONS production over the 1500 pulses simulated are shown in figure 2. The RONS can be divided into two categories: the long-lived RONS that accumulate over the duration of the discharge (figure 2(a)) and the short-lived RONS whose densities oscillate as the plasma is pulsed (shown in figure 2(b) over the last pulse). The long-lived RONS include O_3 , NO_2 , NO_3 , N_2O , and N_2O_5 , while the short-lived RONS are O , N , and, to some extent, NO . The long-lived RONS accumulate over the first 20 ms. The most abundant RONS is O_3 with a density of $2.1 \times 10^{17} \text{ cm}^{-3}$ at 150 ms. O_3 is formed by



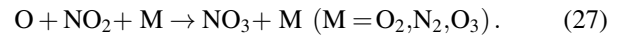
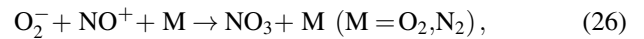
Several nitrous oxide species, N_xO_y , are also formed in the discharge. N_2O is primarily formed by



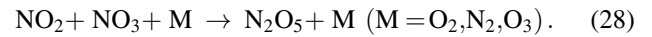
Over the last pulse, NO_2 is formed by



NO_3 is formed by



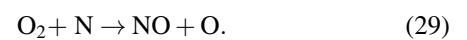
N_2O_5 is formed by



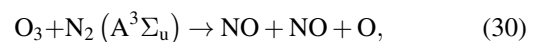
As NO_2 and NO_3 are required to form N_2O_5 , the density of N_2O_5 increases after several hundreds of pulses after formation of the precursors.

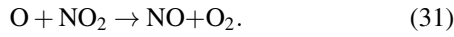
O_3 production for water purification is energy intensive, and so maximizing efficiency is a high priority. Comparison can be made of computed characteristics of this device to experimental devices described in the literature. The residence time of gas for our device is about 16 ms, which corresponds to when the majority of RONS densities achieve a steady state in the absence of the surface reaction mechanism. The energy deposition after 16 ms is 137 mJ cm^{-3} . For an O_3 density of $1.4 \times 10^{17} \text{ cm}^{-3}$ at 16 ms, this energy deposition equates to a production efficiency of $6.1 \text{ eV/O}_3\text{-molecule}$ or production yield of 294 g kWh^{-1} . DBDs described in the literature operated in pure O_2 have similar efficiencies, ranging from 150 g kWh^{-1} to 400 g kWh^{-1} [13, 30–33].

The short-lived RONS are produced and consumed at different times during the power pulse as shown in figure 2(b). O and N are both produced during the pulse by electron-impact dissociation of O_2 and N_2 . O and N decrease shortly after the power ramps down as the electron density and T_e decrease, and production by electron-impact reactions decreases. O is consumed primarily in forming O_3 by reaction 20, while N is consumed by formation of NO by

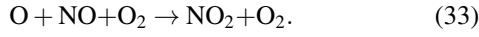
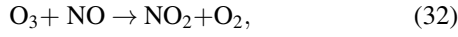


The density of NO increases during the pulse and continues increasing after the pulse, consuming N . Over the last pulse, NO is primarily formed by





The density of NO is maximum at about 9 μs after the pulse and decreases until the next pulse begins. NO is consumed in NO_2 formation, including



3.1. N_2 admixture

The admixture of N_2 in O_2 affects the power deposition into O_2 as well as the RONS produced. As the admixture of N_2 increases, the availability of N increases, increasing the potential for N_xO_y formation.

The variation of the quasi-steady state O_3 density with the added N_2 is shown in figure 3(a). These results are without the surface reaction mechanism. That is, O_3 destruction on surfaces is not included. With the pressure being held constant at 1 atm, adding N_2 decreases the amount of O_2 . With the maximum N_2 added being 10%, the decrease in O_2 is at most 10%. As the N_2 percentage increases, the O_3 density monotonically decreases. The decrease in O_2 density has some effect on O_3 production but is not the major cause for the decrease in O_3 density. There are two reasons for the decrease in O_3 density: O availability and N_xO_y production.

As N_2 percentage increases, the maximum O density produced during the discharge pulse decreases. This decrease in O production is due to power being channeled into N_2 instead of O_2 , as shown in figure 3(b). As the N_2 percentage increases, the power channeled into N_2 linearly increases; however, this increase occurs at a rate twice that of the N_2 increase. For example, at 0.5% N_2 , the power deposited into N_2 is 1%. This occurs because N_2 has higher cross-sections for excitation of vibrational and electronic states than the cross-sections for corresponding states in O_2 . The decrease in power going into O_2 leads to a decrease in maximum O density by 25% from 0% N_2 to 10% N_2 . The power going into N_2 leads to more N atom availability, increasing linearly with N_2 percentage to reach a maximum of $4.1 \times 10^{12} \text{ cm}^{-3}$ over the last pulse at 10% N_2 . The increased availability of N leads to formation of nitrous oxides N_xO_y . N_xO_y formation further consumes O that would otherwise be available for O_3 production, and therefore also contributes to the decrease in O_3 density.

3.2. Gas temperature

The density of O_3 produced in DBDs is strongly dependent on gas temperature T_g due to rates of formation and destruction of O_3 being dependent on temperature. The reactions and rate coefficients responsible for O_3 production are

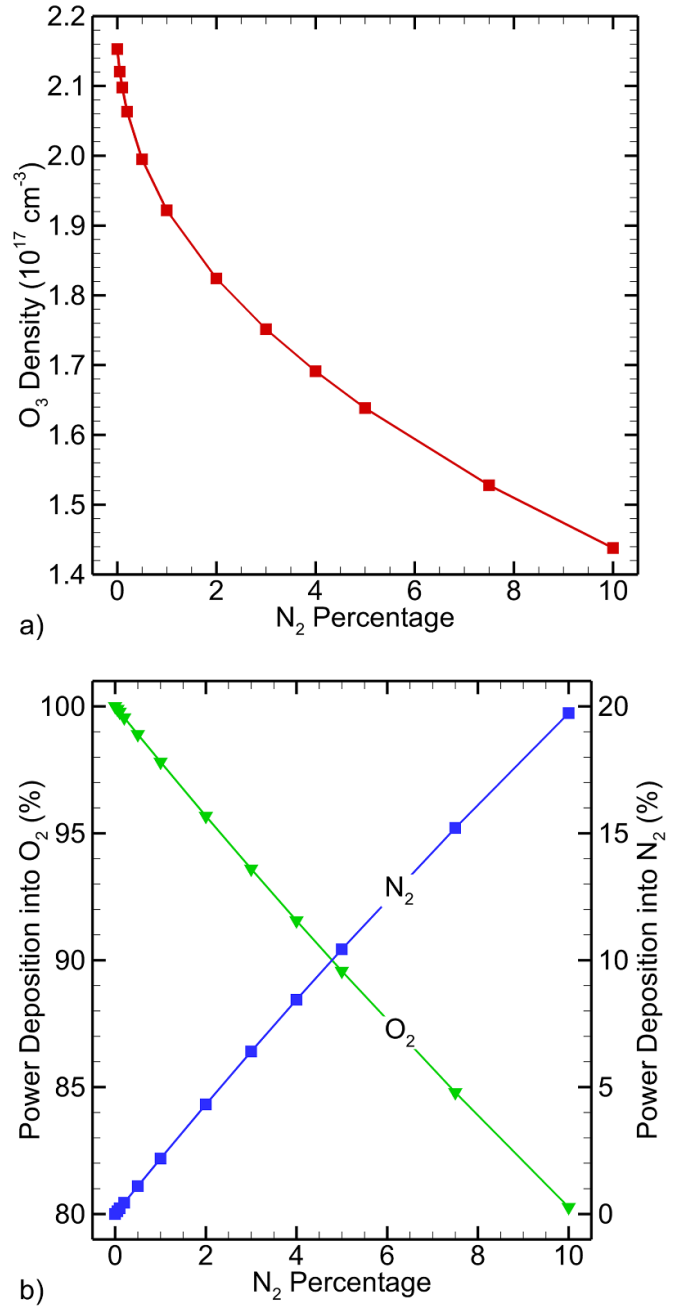
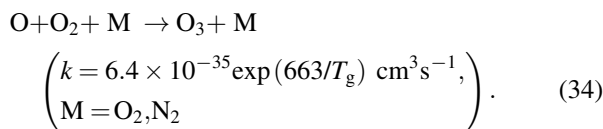


Figure 3. Plasma properties for the O_2 DBD as function of N_2 additive. (a) O_3 density. (b) Power deposition into O_2 and N_2 . Reactions on the surface are not included.



$$\left(k = 1.3 \times 10^{-34} \exp(663/T_g) \text{ cm}^3 \text{ s}^{-1}, \right. \\ \left. \text{M} = \text{O}_3 \right). \quad (35)$$

These rate coefficients of O_3 formation decrease with increasing T_g . Additionally, as T_g increases, the total gas density decreases to maintain a constant pressure of 1 atm. This decrease in gas density decreases the O_2 available for O_3 formation, as well as the density of the third-body M. The decreasing rate coefficients and gas density decrease the overall rate

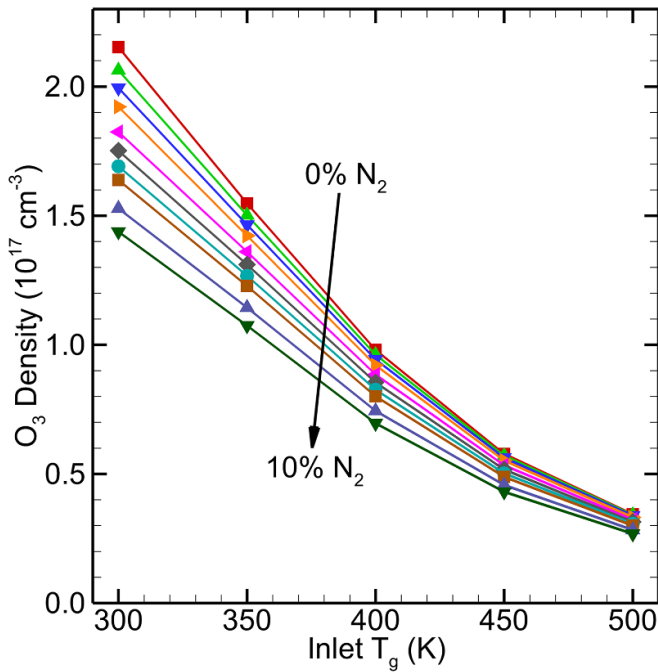
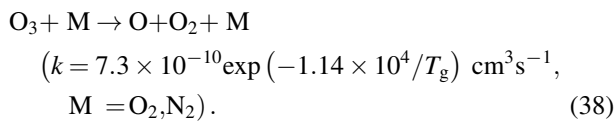
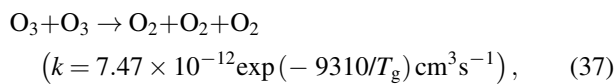
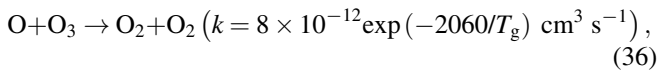


Figure 4. O_3 density as gas and material temperatures vary for different N_2 additive concentrations. Reactions on the surface are not included.

of O_3 formation. At elevated temperatures, O_3 is destroyed in several endothermic reactions with rate coefficients increasing with T_g , including



The rate coefficients of reactions 37 and 38 are small ($< 10^{-19} \text{ cm}^3 \text{ s}^{-1}$) due to the large activation energy required. However, the rate coefficient of reaction 36 ranges from $8.3 \times 10^{-15} \text{ cm}^3 \text{ s}^{-1}$ at 300 K to $1.3 \times 10^{-13} \text{ cm}^3 \text{ s}^{-1}$ at 500 K.

The change in O_3 density with the inlet T_g and wall temperatures varying between 300 K and 500 K was investigated. While T_g in the discharge was solved self-consistently, T_g rose by < 2 K for all inlet T_g investigated. The variation in O_3 density from 300 K to 500 K at different admixtures of N_2 is shown in figure 4. As the rates of O_3 formation decrease and the rates of O_3 destruction increase with T_g , O_3 density decreases as inlet T_g increases. At each admixture of N_2 , the decrease in O_3 density from 300 K to 500 K is at least a factor of 5.

The relative importance of the decrease of formation rate and increase of destruction rates can be understood by studying the 0.2% N_2 case in detail. The decrease in O_3 is primarily due to the decrease in the formation rate, not the increase in the destruction rate because the rate of destruction is at least an order of magnitude smaller than the rate of formation. At 0.2% N_2 , the maximum rate of O_3 formation over the last pulse decreases by a factor of 6 from 300 K to 500 K inlet T_g . This is not due to a lack of atomic O, as the maximum O density over the last pulse actually increases by 5% from 300 K to 500 K. Instead, the decrease in the O_3 formation rate is due to the decrease in the rate coefficient by a factor of 2.4 and a decrease in the gas density by a factor of 1.7 from 300 K to 500 K inlet T_g .

4. Surface destruction of O_3

Reactions of O_3 with surface sites will, in the absence of other effects, generally destroy O_3 . To investigate these processes, simulations were performed with the SKM in *GlobalKin* using the reaction mechanism discussed in section 2 and summarized in table 2. The consequences of the surface reaction mechanism on the gas phase O_3 density, as well as other RONS, is first discussed for an admixture of 0.2% N_2 . The SKM is called every 50 ns and integrated for 1 ms, leading to the evolution of the surface occurring over longer times than integration of gas phase densities. This time-slicing technique enables the surface site densities to come into a steady state within reasonable computation times. Due to the longer integration time of the SKM, the total inventory of N, including in the gas phase and on the surface, increases relative to without surface reactions. This increase reflects the long term adsorption of N species on the surface over times greatly exceeding the residence time of gas in the reactor. The inventory of N in only the gas phase increases by less than 1% due to including surface reactions.

The RONS densities are shown in figure 5(a) (long-lived) and figure 5(b) (short-lived) for 0.2% N_2 . The short-lived RONS densities are shown over the last discharge pulse. O_3 is the most abundant RONS, with a density is $1.9 \times 10^{17} \text{ cm}^{-3}$ at 150 ms. The O_3 density without the surface reaction mechanism (section 3) was $2.1 \times 10^{17} \text{ cm}^{-3}$ at 150 ms. About 10% of the O_3 produced is destroyed on the surface, despite a destruction probability of 0.01. The large amount of O_3 destruction is due to the high surface area to volume ratio (SVR) of the reactor, leading to a short diffusion length of $95 \mu\text{m}$ and a short timescale of diffusion of 0.9 ms. In a gas residence time of 16 ms, the O_3 encounters the wall about 18 times, increasing the likelihood of destruction over the residence time.

The effect of the reactions on the surface can be compared to the effect of gas temperature for 0.2% N_2 . The O_3 density at 150 ms is $1.9 \times 10^{17} \text{ cm}^{-3}$ with the surface reaction mechanism and $3.4 \times 10^{16} \text{ cm}^{-3}$ at 500 K without the surface reaction mechanism. For comparison, without the reactions on the surface at 300 K, the O_3 density at 150 ms is $2.1 \times 10^{17} \text{ cm}^{-3}$. Therefore, the gas temperature can reduce the O_3 density substantially more than surface destruction.

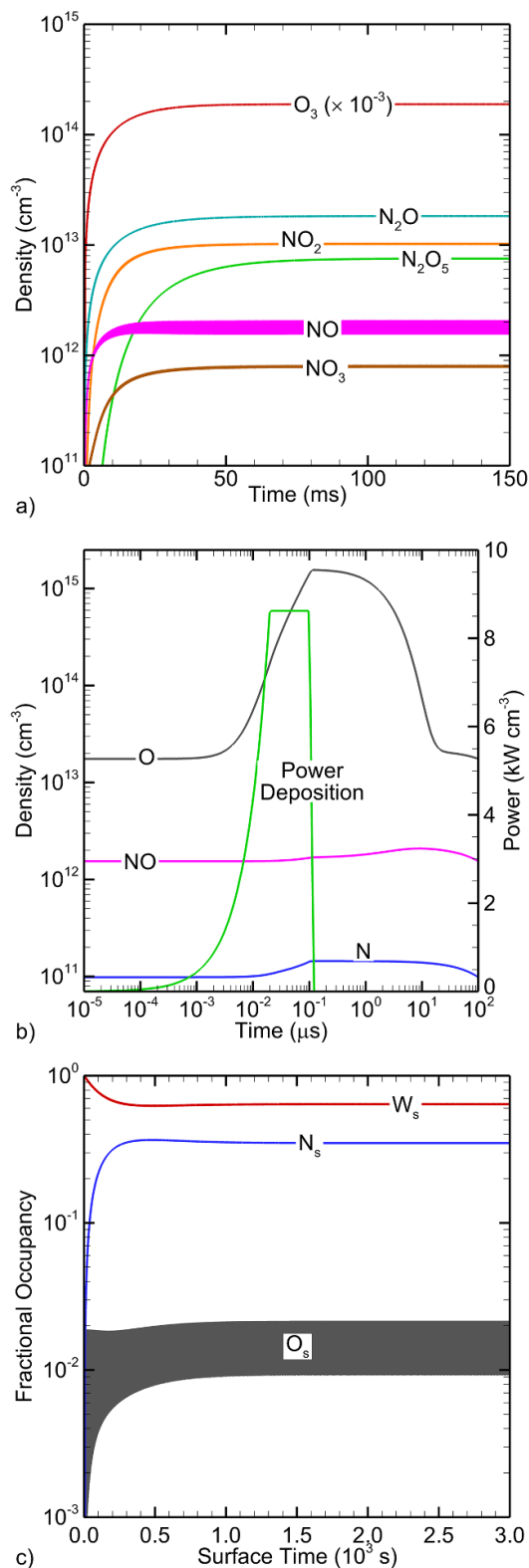


Figure 5. Plasma properties for 0.2% N₂ in O₂ with the surface reaction mechanism. (a) Long-lived reactive species densities, (b) short-lived reactive species densities, and (c) fractional occupancy of surface sites.

The steady state compositions of other RONS are similar with and without the surface reaction mechanism. At 150 ms, NO is increased by 0.2% by the surface reaction

mechanism. This increase occurs because of there being a limited number of reactions consuming NO on the surface. While all these reactions have the same probability, the reaction $O_2 + N_s \rightarrow O_s + NO$ occurs with a higher rate because O₂ is the most abundant molecule in the gas and therefore has the largest flux to the surface. NO₂ is decreased by 9% compared to without surface reactions. NO₂ is more reactive with the surface than NO, being more likely to be destroyed than formed. Production of NO₂ on the surface stems from NO and NO₃. Since NO and NO₃ have lower densities than NO₂ at 150 ms, the rates of production are lower than the rate of NO₂ destruction. NO₃ decreases by 6% compared to without surface reactions. NO₃ is only consumed on the surface and is not produced, decreasing the gas phase concentration of NO₃. N₂O₅ decreases by 16% compared to without surface reactions. The decrease in N₂O₅ is due to the decrease in its precursors, NO₂ and NO₃. N₂O is increased by less than 2% compared to without surface reactions, as N₂O is formed in a surface reaction but is not destroyed on the surface.

The short-lived RONS are shown in figure 5(b) over the last pulse. Compared to without the surface reactions, O in the gas phase is largely unchanged. The maximum density of O decreases by less than 0.3%. In spite of the adsorption of O onto the surface, O_s remains low (<3% of the surface sites). Therefore, the O density is minimally affected by adsorption as production of O from electron-impact dissociation of O₂ is essentially unaffected by the surface mechanism. However, the maximum N density over the last pulse decreases by 31% compared to without surface reactions. This decrease is due to adsorption of N on the surface. Since N₂ is only 0.2% of the gas mixture, this loss of N is not immediately replenished by electron-impact dissociation of N₂ to form N. The decrease in N with and without surface reactions is not as severe at larger N₂ admixtures. With 10% N₂, the decrease in the maximum N in the gas phase is only 2%.

The surface site occupancies are shown in figure 5(c). The gas phase densities come into equilibrium with the surface sites on the order of diffusion times to the surface—at most a few ms—for a given surface composition. (Recall that the surface evolves over longer timescales due to numerical time slicing.) Initially, the surface is covered with empty wall sites W_s. At 3000 s, adsorbed N_s occupies 35% of the surface sites, while empty wall sites W_s comprise 64% of the surface. The decrease in W_s is largely due to the increase in N_s. With this high site occupancy, N_s blocks some of the W_s that could otherwise destroy O₃ through $O_3 + W_s \rightarrow O_s + O_{2s}$. O_s occupies 0.9% of the surface sites. O_{2s} and N_{2s} occupy less than 0.1% of the surface as their binding energies are small and they are removed from the surface by collisions with O₂. Even with a low probability of desorption, the flux of O₂ is high, and O_{2s} and N_{2s} are rapidly removed.

Despite N_s and O_s having the same adsorption and recombination probabilities, their surface occupancies are very different. O_s has a much lower surface occupancy than N_s, because the removal rates of O_s are higher than the removal rates of N_s. Both N_s and O_s can be removed from the surface by O₂; however, O_s is removed in O₃ formation (reaction 10) with a probability of 0.004, while N_s is removed in NO formation

(reaction 13) with a probability of 10^{-8} . O_s is also removed from the surface in O_3 destruction (reaction 6). The probability of O_3 destruction by O_s is 0.01, while the other reactions that remove N_s from the surface have probabilities of 10^{-8} . O_s also experiences more oscillation than N_s . While the rates of removal of O_s by O_3 and O_2 remain constant over the pulse, other reactions that adsorb or remove O_s do not. O_s is adsorbed while O is present during or shortly following the pulse, while O_s is removed by recombination to form O_2 . While these same adsorption and desorption mechanisms exist for N_s , N_s has a much higher occupancy and is not as affected by the dynamics over one pulse.

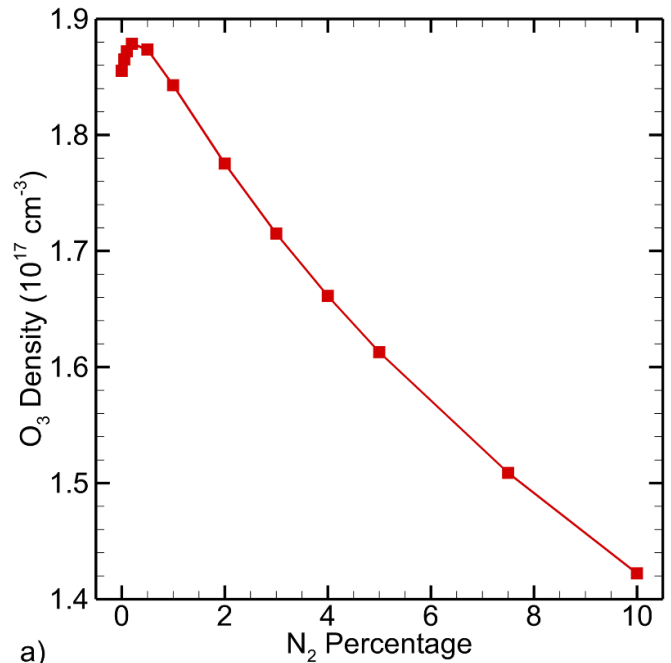
4.1. N_2 admixtures

A monotonic decrease in O_3 density with increasing N_2 occurred without considering surface reactions. However, with the reactions on the surface, increasing N_2 admixture changes the surface occupancies and, therefore, the destruction of O_3 occurring on the surface.

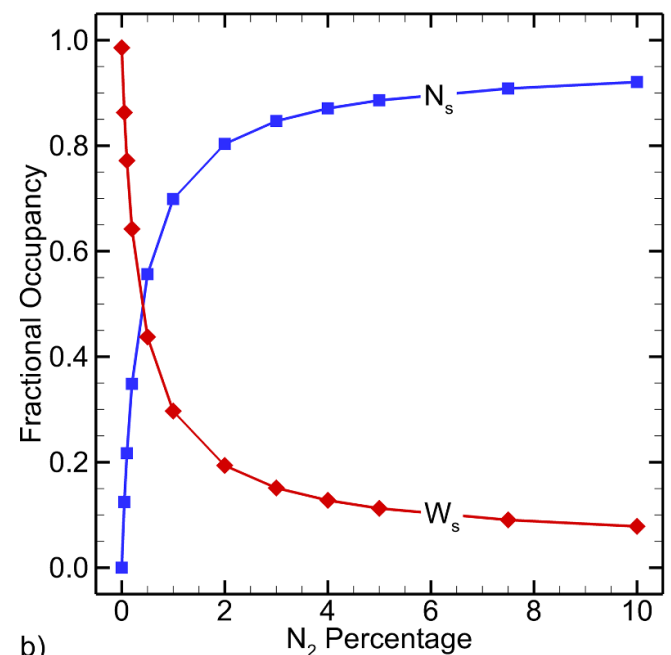
The effect of N_2 admixture on O_3 density when including the surface reaction mechanism is shown in figure 6(a). The trend in O_3 density is no longer a monotonic decrease in O_3 with increasing N_2 . The O_3 density increases from 0% N_2 to 0.2% N_2 prior to decreasing with further increase in N_2 percentage. The increase in the O_3 density at N_2 admixtures below 0.2% is explained by the surface occupancies, shown in figure 6(b). O_3 is destroyed by reactions on the surface with W_s and adsorbed O_s . O_s at the end of the simulation is below 1.5% of the surface sites for all N_2 percentages, while W_s occupies at least 7% of the surface sites for all N_2 percentages. Therefore, O_3 is mostly destroyed in reactions with W_s . The surface occupancy of W_s decreases as N_2 percentage increases corresponding to an increase in sites with adsorbed N_s . Therefore, N_s occupies surface sites that would otherwise be available for O_3 destruction.

Based solely on the increase of N_s and decrease of O_3 destruction on the surface, O_3 density would be expected to increase as N_2 admixture increases. However, above 0.2% N_2 , the density of O_3 decreases. This decrease occurs because more power is deposited into N_2 compared to O_2 as the N_2 percentage increases as discussed in section 3.1. Therefore, less O is produced in the gas phase. O can also be diverted from O_3 production to form N_xO_y species, further decreasing the O_3 density. The competition between decreased surface destruction of O_3 and increased power into N_2 as N_2 percentage increases creates a maximum in O_3 at 0.2% N_2 .

Experimental observations have shown that even after the N_2 flow has been turned off, the O_3 percentage remains elevated for some period of time before decreasing [11, 12]. The surface mechanism can reproduce this behavior. A simulation was initialized with the species densities and surface occupancies at the end of the 0.2% N_2 case, and only O_2 was flowed into the reactor. The O_3 density decreased as the N_s was removed from the surface by desorption or reactions to form N_xO_y species. At 1000 s of surface reactivity, N_s was reduced to 7% of the surface sites from its initial value of 35%. The O_3 density after 1500 pulses of pure



a)



b)

Figure 6. Plasma properties with the surface reaction mechanism as a function of N_2 additive in O_2 . (a) O_3 density and (b) fractional occupancy of surface sites.

O_2 flowing into the reactor (50 min of surface reactivity) decreased from $1.92 \times 10^{17} \text{ cm}^{-3}$ (steady state value at 0.2% N_2) to $1.86 \times 10^{17} \text{ cm}^{-3}$, matching the O_3 density at 0% N_2 .

4.2. Probability of O_3 destruction

The probability of O_3 destruction on the surface directly affects the O_3 density in the reactor. As the precise values of probabilities of these destruction processes are not well

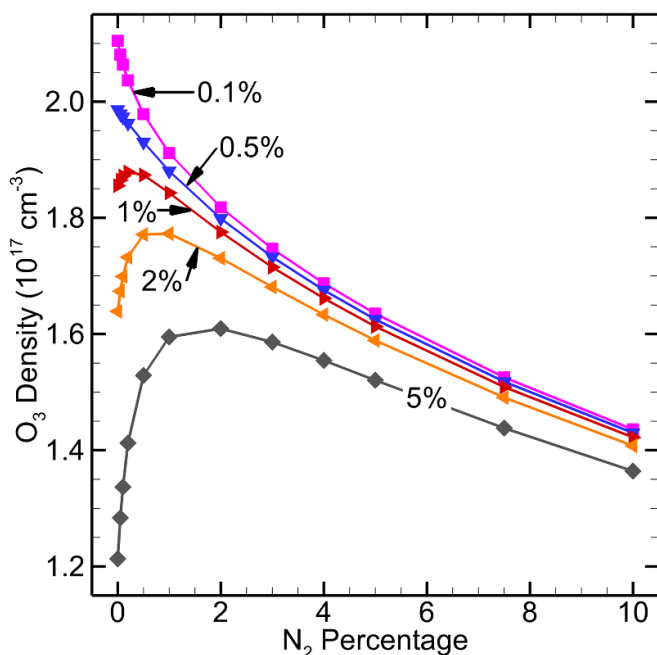
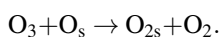
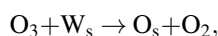


Figure 7. O_3 density as a function of N_2 additive for different surface destruction probabilities of O_3 .

known, the probabilities of O_3 destruction were varied in reactions 5 and 6,



The O_3 densities at different destruction probabilities and N_2 admixtures are shown in figure 7. As expected, the O_3 density decreases as the surface destruction probability increases. This decrease occurs simply because more O_3 is being destroyed on the surface. At 0.2% N_2 and a probability of 0.01 for O_3 destruction, the O_3 density is $2.0 \times 10^{17} \text{ cm}^{-3}$, only slightly lower than without the surface reactions ($2.1 \times 10^{17} \text{ cm}^{-3}$). This decrease, even at low destruction probabilities, occurs because the reactor has a high SVR and O_3 encounters the surface many times before flowing out of the reactor.

In addition to the decrease in O_3 density with increasing surface destruction probability, the admixture of N_2 where the O_3 density is maximum increases with increasing destruction probability. At probabilities of O_3 destruction of 0.001 and 0.005, the O_3 density is maximum at essentially 0% N_2 , matching the results when reactions on the surface are not considered. This maximum at 0% N_2 is due primarily to the low amount of O_3 destruction on the surface. The maximum in O_3 density shifts to 0.2% N_2 at 0.01 destruction probability. At 0.02 destruction probability, the maximum in O_3 density shifts to 1% N_2 , and at 0.05 destruction probability, the maximum in O_3 further shifts to 2% N_2 . This shift in the N_2 percentage where the O_3 density is maximum is due to the need for N atoms to occupy a larger fraction of surface sites, blocking O_3 destruction processes, when the destruction probability

increases. In spite of there being more power being channeled into N_2 with increasing N_2 percentage, the benefit of blocking sites where O_3 destruction can occur at higher rates is more beneficial. Increasing N_2 percentage increases the rate of production of N atoms that block the sites.

4.3. Surface roughness

The roughness of the dielectric surface can vary between different reactors by choice of materials and materials processing, and during the lifetime of the reactor. The surface roughness will affect several of the model parameters, including reaction rates. In the context of this study, the roughness of the surface is represented by the surface site density and the net surface occupancy. A plane-view of a rough surface has more surface sites per unit area than smooth surfaces.

The O_3 density and N_s fractional occupancy are shown in figures 8(a) and (b), respectively, for different surface site densities—higher surface site densities correspond to rougher surfaces. The probability of destruction of O_3 on the surface is 1%. At 0% N_2 , the O_3 density is essentially the same for all surface site densities. Since increasing the site density does not decrease the O_3 density, the flat-surface site density of 10^{15} cm^{-2} is sufficient to interact with the O_3 that diffuses to the wall. With increasing N_2 percentage, power is diverted from O_2 which creates O atoms to N_2 . The benefit of N_2 then comes from N adsorption on surface sites. With a larger number of surface sites that occurs with increasing roughness, the likelihood for O_3 destruction increases. However, for a fixed power, the production of N atoms is fixed (and independent of surface roughness). There are not enough N atoms being produced (and adsorbed) to offset the increased likelihood for O_3 destruction. N_s does block some empty W_s sites that could otherwise destroy O_3 . However, the occurrence of unblocked sites increases more rapidly than sites occupied by N_s as the total site density increases.

While the overall O_3 density decreases with increasing surface site density, the N_2 admixture where there is some benefit to O_3 density occurs also shifts. The N_2 admixture where the maximum in O_3 density occurs decreases with surface roughness. At a site density of 10^{15} cm^{-2} the maximum in O_3 density occurs at 0.2% N_2 . At a site density of $2 \times 10^{15} \text{ cm}^{-2}$, the maximum in O_3 density shifts to 0.1% N_2 and shifts further to 0.05% N_2 at a site density of $3 \times 10^{15} \text{ cm}^{-2}$. At a site density of $5 \times 10^{15} \text{ cm}^{-2}$, the maximum in O_3 density occurs at 0% N_2 . The benefit of N_2 admixtures is small due to the higher rates of O_3 quenching on the larger number of surface sites.

As discussed above, the benefit of the N_2 admixture increases with increasing probability of quenching O_3 . The higher the destruction probability, the greater the benefit of N_s blocking a site that can destroy O_3 . The variation in O_3 density is shown in figure 8(c) for different surface site densities for higher surface destruction probability of O_3 of 0.02. Similar to the 0.01 surface destruction probability of O_3 , the O_3 density decreases with increasing surface site density, and the N_2 admixture where the maximum in O_3 density occurs decreases. However, the decrease is more pronounced. For a site density of 10^{15} cm^{-2} , the maximum O_3 density occurs at

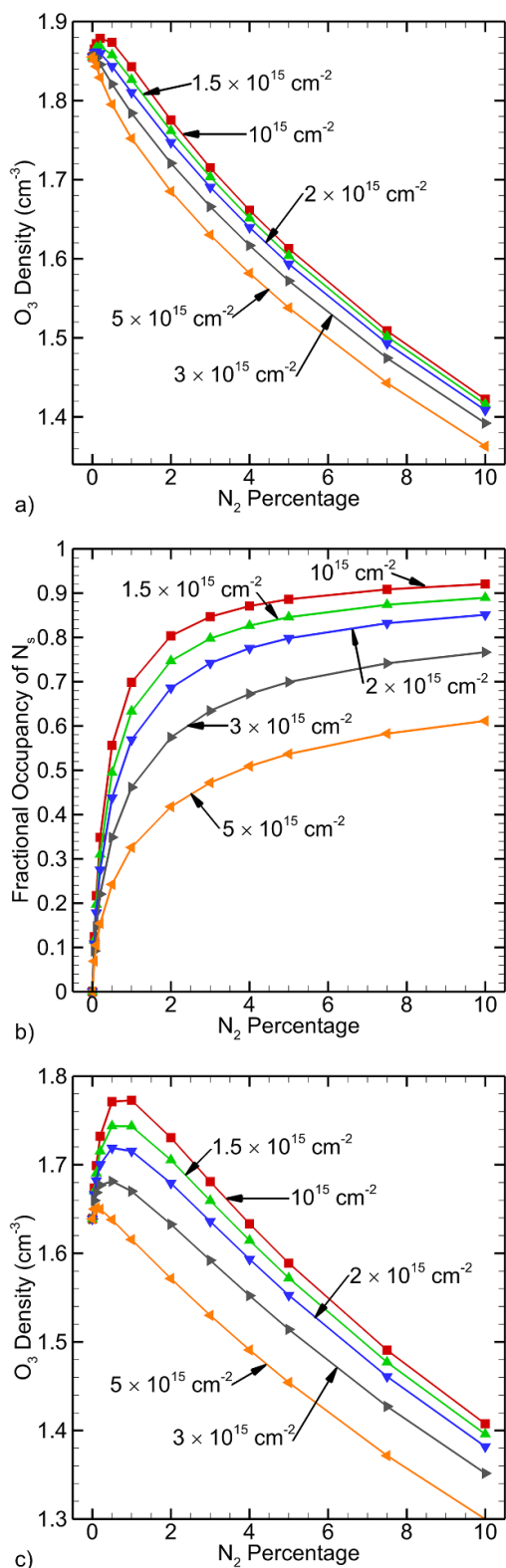


Figure 8. Plasma and surface properties as a function of N_2 additive in O_2 for different surface site densities (approximating surface roughness). (a) O_3 density and (b) fractional occupancy of surface sites for 0.01 surface destruction probability of O_3 . (c) O_3 density for 0.02 surface destruction probability of O_3 .

1% N_2 and decreases to 0.1% N_2 for a surface site density of $5 \times 10^{15} \text{ cm}^{-2}$.

5. Concluding remarks

O_3 destruction on the walls of DBD reactors has been hypothesized to be the cause of the OZP. Addition of N_2 into an otherwise pure O_2 discharge has been shown to suppress the OZP and increase O_3 concentration, despite the discharge power that is diverted from O_2 into N_2 and the corresponding increase in N_xO_y species. A general surface reaction mechanism including destruction of O_3 on the surface was proposed in this work to explain the increase in O_3 concentration at nonzero admixtures of N_2 . The general surface reaction mechanism was coupled to a global plasma chemistry model, and a DBD having a high SVR was simulated for 1500 discharge pulses corresponding to 50 min of surface evolution.

The results of the simulation were first analyzed without including O_3 destruction on the surface. The O_3 concentration decreases when the admixture of N_2 increases. This decrease is due to a decrease in the power deposited into O_2 and a corresponding increase in the power deposited into N_2 , in addition to formation of nitrogen oxides consuming O that could otherwise form O_3 . When the inlet gas temperature is increased, the O_3 density steadily decreases as the rate of O_3 formation decreases at elevated temperatures.

The reactions on the surface, including O_3 destruction, were then included in the simulation. The overall O_3 density decreases due to its destruction on surfaces, while most other RONS have a similar concentrations. For an O_3 destruction probability of 0.01, increasing the admixture of N_2 increases the O_3 density up an addition of 0.2% N_2 and then decreases the O_3 density at higher N_2 admixtures. The increase at low N_2 admixtures is due to N_s occupying surface sites that otherwise might be used for O_3 destruction. The decrease at higher N_2 admixtures is due to less power being deposited into O_2 and formation of N_xO_y . The maximum at 0.2% N_2 agrees qualitatively with previously published results, where O_3 concentration was boosted with 0.2%–4% N_2 dependent on the reactor geometry.

The O_3 density decreases as the probability of surface destruction increases. However, a significant fraction of this O_3 loss can be recovered by adding N_2 . For example, for an O_3 destruction probability of 0.05, about half of the loss can be recovered by N_2 addition of about 2%. For these conditions, the benefit of removing quenching sites for O_3 by occupying those sites with N_s outweighs the loss incurred by power flowing into N_2 . As surface roughness increases, O_3 concentration generally decreases due to there being more sites for O_3 loss. Some of this loss can be recovered by N_s passivation. However, the N flux to the surface must increase in greater proportion than the increase in site density.

O_3^* , a vibrationally excited state of O_3 was not included in mechanism due to its low fluxes to surfaces at atmospheric

pressure. O_3^* has a large quenching coefficient to the ground state on surfaces [34] while we expect O_3^* will be more likely to dissociate on surfaces due to its lower activation energy for this process. If this expectation is met, then conditions which produce larger fluxes of O_3^* to surfaces will also likely enhance the beneficial effect of N_2 addition on net ozone production.

The surface reaction mechanism proposed is general. Probabilities of reactions on the surface were taken for borosilicate glass, a common dielectric, where possible and were otherwise estimated to explain the increase in O_3 density at nonzero N_2 admixtures. The reactions on the surface and their associated probabilities will vary depending on the material in contact with the plasma. The surface composition of the materials in contact with the plasma could change with increasing plasma exposure, processes that were not considered in this investigation. Metal electrodes could oxidize, changing the probabilities of reactions on the surface as the surface composition changes over the reactor lifetime. Catalytic materials could change the reactions occurring on the surface. However, the trends discussed here can help guide selection of materials to decrease the OZP. Based on our results, materials should have, as first order, low surface destruction probability of O_3 , high rates of adsorption of N, and low surface roughness to help suppress the OZP.

Data availability statement

The data that support the findings of this study are included in this article and available from the corresponding author upon reasonable request.

Acknowledgments

This work was supported by the National Science Foundation (CBET 2032604). This material was also based upon work supported by the U.S. Department of Energy, Office of Science, Office of Fusion Energy Sciences under Award No. DE-SC0020232.

Conflict of interest

The authors have no conflicts of interest to disclose.

ORCID iDs

Mackenzie Meyer  <https://orcid.org/0000-0002-2105-6690>

John Foster  <https://orcid.org/0000-0001-8369-1828>

Mark J Kushner  <https://orcid.org/0000-0001-7437-8573>

References

- [1] Adamovich I et al 2022 *J. Phys. D: Appl. Phys.* **55** 373001
- [2] Foster J E 2017 *Phys. Plasmas* **24** 055501
- [3] Foster J E, Mujovic S, Groele J and Blankson I M 2018 *J. Phys. D: Appl. Phys.* **51** 293001
- [4] Itoh H, Suzuki T, Suzuki S and Rusinov I M 2004 *Ozone Sci. Eng.* **26** 487
- [5] Yanallah K, Hadj Ziane S and Belasri A 2006 *Plasma Devices Oper.* **14** 215
- [6] Mazánková V, Trunec D, Krzyžánková A, Jurmanová J and Krčma F 2020 *Jpn. J. Appl. Phys.* **59** SHHA02
- [7] Taguchi M, Yamashiro K, Takano T and Itoh H 2007 *Plasma Process. Polym.* **4** 719
- [8] Murayama K, Matsumura N, Taguchi M, Katoh Y, Teranishi K, Suzuki S and Itoh H 2009 *EPJ Appl. Phys.* **47** 22814
- [9] Taguchi M, Ochiai Y, Kawagoe R, Kato Y, Teranishi K, Suzuki S and Itoh H 2011 *EPJ Appl. Phys.* **55** 13805
- [10] Itoh H, Nagai T, Taguchi M, Teranishi K and Suzuki S 2021 *Plasma Res. Express* **3** 035001
- [11] Seyrling S, Müller M and Ramoino L 2017 *Eur. Phys. J. D* **71** 136
- [12] Seyrling S, Reisch E and Ramoino L 2018 *Ozone Sci. Eng.* **40** 356
- [13] Qin Y, Qian S, Wang C and Xia W 2018 *Plasma Sci. Technol.* **20** 095501
- [14] Lietz A M and Kushner M J 2016 *J. Phys. D: Appl. Phys.* **49** 425204
- [15] Bhoj A N and Kushner M J 2007 *J. Phys. D: Appl. Phys.* **40** 6953
- [16] Polito J, Denning M, Stewart R, Frost D and Kushner M J 2022 *J. Vac. Sci. Technol. A* **40** 043001
- [17] Van Gaens W and Bogaerts A 2013 *J. Phys. D: Appl. Phys.* **46** 275201
- [18] Atkinson R, Baulch D L, Cox R A, Hampson R F, Kerr J A and Troe J 1997 *J. Phys. Chem. Ref. Data* **26** 1329
- [19] Atkinson R, Baulch D L, Cox R A, Hampson R F, Kerr J A and Troe J 1997 *J. Phys. Chem. Ref. Data* **26** 521
- [20] Mellouki A, Poulet G and Le Bras G 1987 *J. Geophys. Res.* **92** 4217
- [21] London G, Gilpin R, Schiff H I and Welge K H 1971 *J. Chem. Phys.* **54** 4512
- [22] Gordiets B F, Ferreira C M, Guerra V L, Loureiro J M A H, Nahorny J, Pagnon D, Touzeau M and Vialle M 1995 *IEEE Trans. Plasma Sci.* **23** 750
- [23] Laher R R and Gilmore F R 1990 *J. Phys. Chem. Ref. Data* **19** 277
- [24] Kramida A, Ralchenko Y and Reader J NIST Atomic Spectra Database 2022 (Gaithersburg, MD: National Institute of Standards and Technology)
- [25] Li W, Gibbs G V and Oyama S T 1998 *J. Am. Chem. Soc.* **120** 9041
- [26] Stafford L, Guha J and Donnelly V M 2008 *J. Vac. Sci. Technol. A* **26** 455
- [27] Macko P, Veis P and Cernogora G 2004 *Plasma Sources Sci. Technol.* **13** 251
- [28] Kutasi K and Loureiro J 2007 *J. Phys. D: Appl. Phys.* **40** 5612
- [29] Guerra V, Marinov D, Guaitella O and Rousseau A 2014 *J. Phys. D: Appl. Phys.* **47** 224012
- [30] Homola T, Prukner V, Hoffer P and Šimek M 2020 *Plasma Sources Sci. Technol.* **29** 095014
- [31] Jodzis S and Zięba M 2018 *Vacuum* **155** 29
- [32] Li M, Zhu B, Yan Y, Li T and Zhu Y M 2018 *Plasma Chem. Plasma Process.* **38** 1063
- [33] Šimek M, Pekárek S and Prukner V 2010 *Plasma Chem. Plasma Process.* **30** 607
- [34] Marinov D, Guerra V, Guaitella O, Booth J-P and Rousseau A 2013 *Plasma Sources Sci. Technol.* **22** 055018
- [35] Cartry G, Magne L and Cernogora G 2000 *J. Phys. D: Appl. Phys.* **33** 1303
- [36] Janssen C and Tuzson B 2010 *J. Phys. Chem. A* **114** 9709